Supplement of Atmos. Chem. Phys., 19, 901–919, 2019
https://doi.org/10.5194/acp-19-901-2019-supplement

Atmospheric Chemistry and Physics
Open Access
EGU

Supplement of

Sources and processes that control the submicron organic aerosol composition in an urban Mediterranean environment (Athens): a high temporal-resolution chemical composition measurement study

Iasonas Stavroulas et al.

Correspondence to: Aikaterini Bougiatioti (abougiat@noa.gr) and Nikolaos Mihalopoulos (nmihalo@noa.gr)

S1 ACSM Calibration

Measuring Period	RF NO_3^-	RIE NH_4^+	RIE $SO_4^=$
Winter 2013-2014	$5.91e^{-11}$	4.5	0.6
Winter 2015-2016	$5.63e^{-11}$	5.15	0.48
2016-2017	$4.61e^{-11}$	4.8	0.58

Table S.1: Response factor and relative ionization efficiencies determined for the different measuring periods

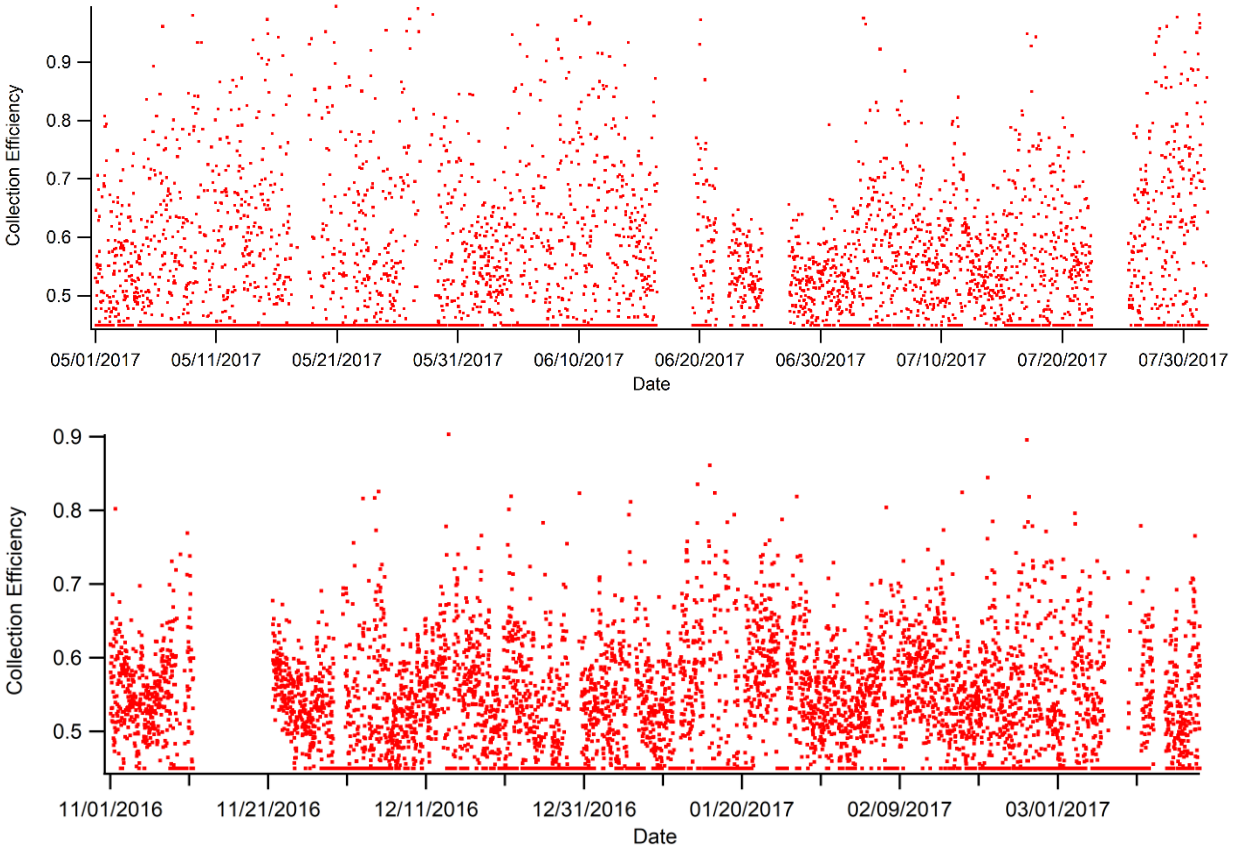

Figure S1. Collection efficiencies applied to the ACSM datasets indicativelly for the warm period of 2017 and the cold period of 2016 – 17 according to

S2 Meteorological Parameters

An overview of the prevailing meteorological conditions, regarding the yearlong period of measurements 2016 – 2017 is presented in terms of diurnal variability below.

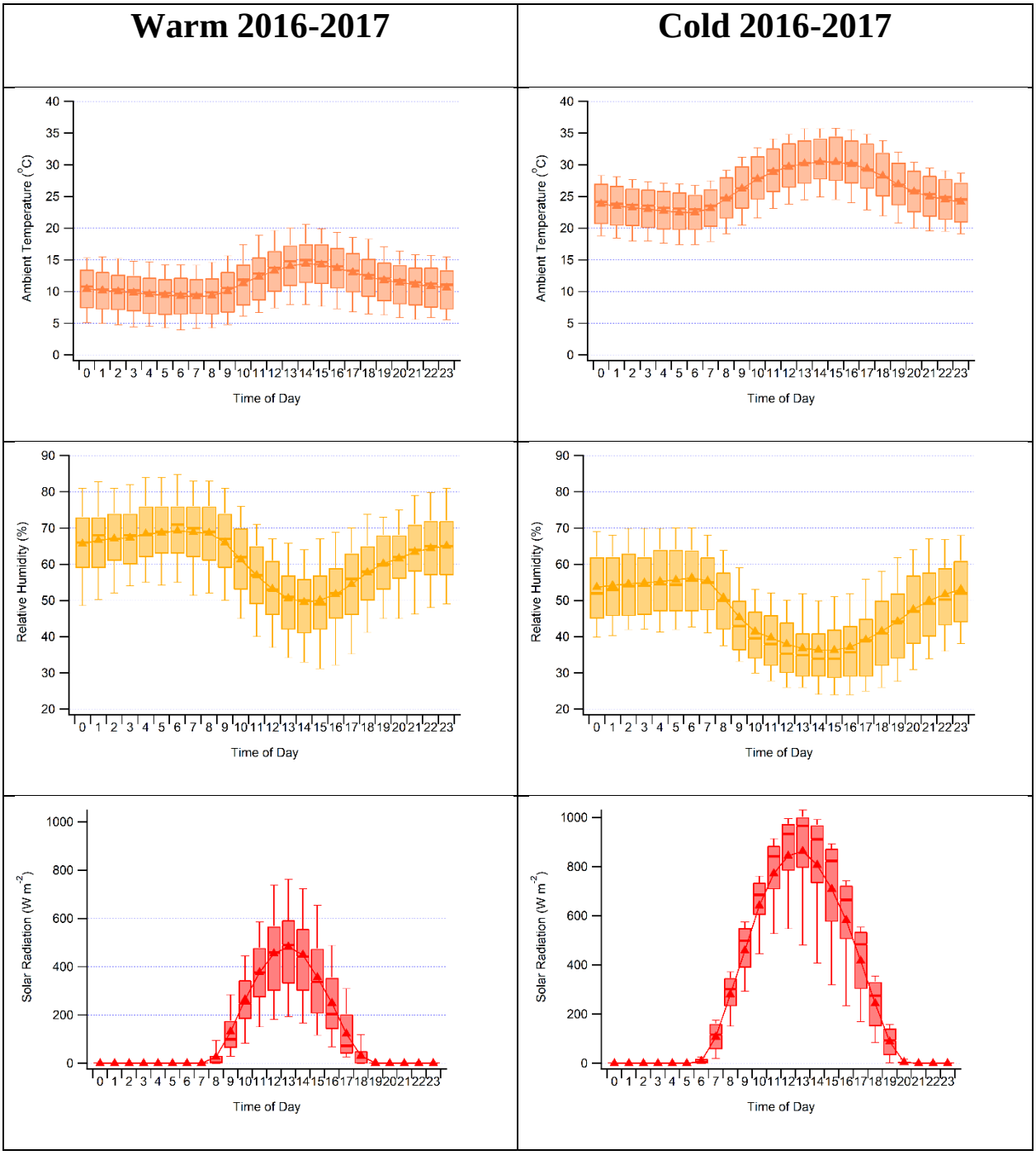

Figure S2. Diurnal variability during the cold versus warm season for ambient temperature (top), relative humidity (middle) and solar irradiance (bottom).

S.3 ACSM Quality Assurance/ Quality Control

As a first quality control/quality assurance of the obtained data, ammonium concentrations obtained by the ACSM are compared to the respective ammonium concentrations derived from the PILS, both for winter 2016-17 as well as winter 2013-2014. Both measurements are averaged hourly for synchronization reasons. The respective graphs are given in the following figures (Figure SI.1.1, SI.1.2). Furthermore, ACSM concentrations are daily-averaged and the derived averages are compared to the respective concentrations obtained by ion chromatography analysis and thermal-optical analysis of the respective daily $PM_{2.5}$ filters for all the winter periods (Figure SI.1.1, SI.1.2).

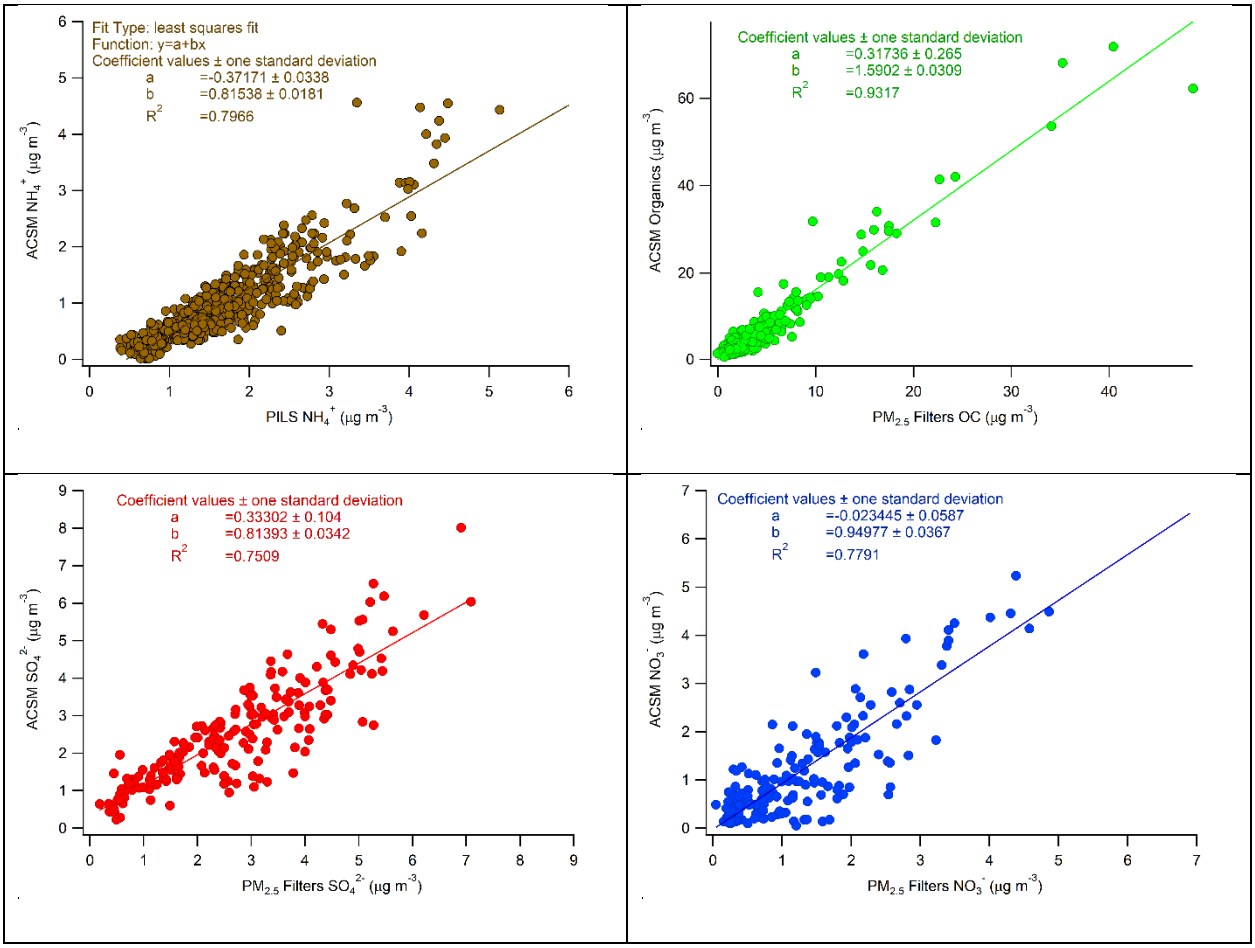

Figure S3. Correlations of the non-refractory PM_1 constituents as measured by the ACMS versus external measurements for the year-long period 2016-2017. Top left ammonium from ACSM vs PILS measurements, top right ACSM Organics vs OC measured on filters using a thermal optical method, bottom left ACSM sulfate vs IC sulfate and bottom left ACSM nitrate vs IC nitrate.

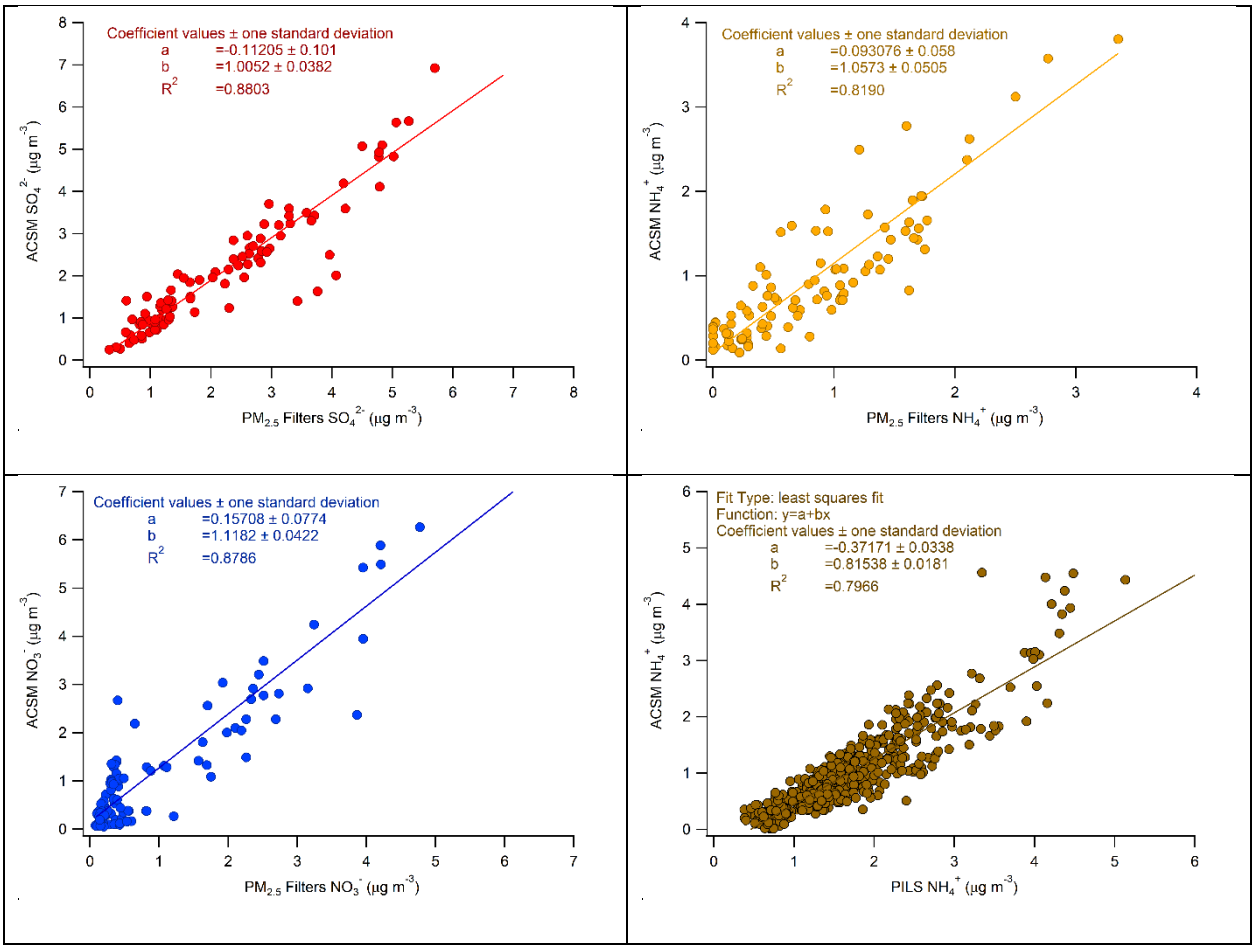

Figure S4. Correlations of the non-refractory PM_1 constituents as measured by the ACMS versus external measurements for the wintertime intensive campaigns of 2013-2014 and 2015-2016. Top left ACSM sulfate vs IC sulfate (2015-2016), top right ACSM ammonium vs IC ammonium (2015-2016), bottom left ACSM nitrate vs IC nitrate (2015-2016) and bottom right ACSM ammonium vs PILS ammonium (2013-2014)

The instrument has participated in an intercomparison study of 15 Q-ACSM instruments organized by the European Center for Aerosol Calibration (ECAC) at the Aerosol Chemical Monitor Calibration Center (ACMCC) at Site Instrumental de Recherche par Télédétection Atmosphérique (SIRTA, Paris) during March 2016 (www.actris-ecac.eu/acsm-2016-1.html). It showed excellent agreement (well below ±20%) with the ACMCC's reference instrument, in both pre- and post-calibration periods of the intercomparison study, while the relative ionization efficiencies (RIE) for ammonium and sulfate, obtained by the on-site calibration, were very close to the ones previously used, indicating a stable performance of the instrument.

S4 Source Apportionment of OA

The source apportionment procedure is presented for the cold season of 2016 – 2017 and for the warm season of 2017, which are discussed in the manuscript.

S4.1 Anchor profiles

The spectra used as RFPs are ambient deconvolved mass spectra found in the AMS spectral database (Ulbrich et al., 2009; Ulbrich et al., 2013). Specifically, the HOA and BBOA factors were constrained using the RFPs derived from multiple datasets in the study of Ng et al. (2011b), while the anchor FP used for the COA factor was deconvolved during a study in Paris by Crippa et al. (2013). Representativeness of the selected RFPs is assessed by comparison to factors reported in earlier studies in the region and the relevant coefficients of determination can be seen in figures SF.15 through SF.17. For the HOA RFP, values for r^2>0.95 were calculated when comparing to HOA factors from Athens, Patras and Bologna (Florou et al., 2017; Kostenidou et al., 2015; Gilardoni et al., 2016), COA RFP exhibited excellent correlation with spectra for Athens and Patras (r^2>0.9) (Florou et al., 2017), while BBOA showed excellent correlation ($r^2>0.87$) with spectra obtained earlier in urban areas in the region (Florou et al., 2017; Gilardoni et al., 2016) as well as in the regional background site at Finokalia (Bougiatioti et al., 2014) (r^2=0.79).

S4.2 Unconstrained runs

As stated in step 1 of the SA methodology proposed by Crippa et al. (2014), an unconstrained run (PMF) was first performed in the split data sets. A discussion of the PMF findings for each period follows.

Cold Period 2016-2017: The 4 and 5 factor solution PMF (unconcstrained) runs for this period are displayed in Figure SF.5. For the 4 solution PMF runs we can distinguish an HOA-like factor at position 1, a BBOA-like factor in position 3, an OOA like factor in position 2, and what could be a COA-like factor in position 4. Small seed variability was observed for the four factor solution. Nevertheless, the model produced residuals exhibiting a clear diurnal structure for several variables (e.g. m/z 43, 51, 53, 55, 57) with a maximum during the morning traffic rush hour, as can be seen indicatively in the lower panel of Figure SF.5 for m/z=55. This fact led us to the exploration of the 5 factor PMF solution which is presented in the top left panel of Figure SF.5. The issue in the residual structure is mitigated when going through the 5 factor solution, where the model seems to be able to predict the OA behavior during the traffic rush hour, exhibiting no residual structure in the fragments associated with primary HOA. Nevertheless, FPs vary considerably for different seed runs leading to the exploration of a constrained five factor run in the next step of the SA procedure.

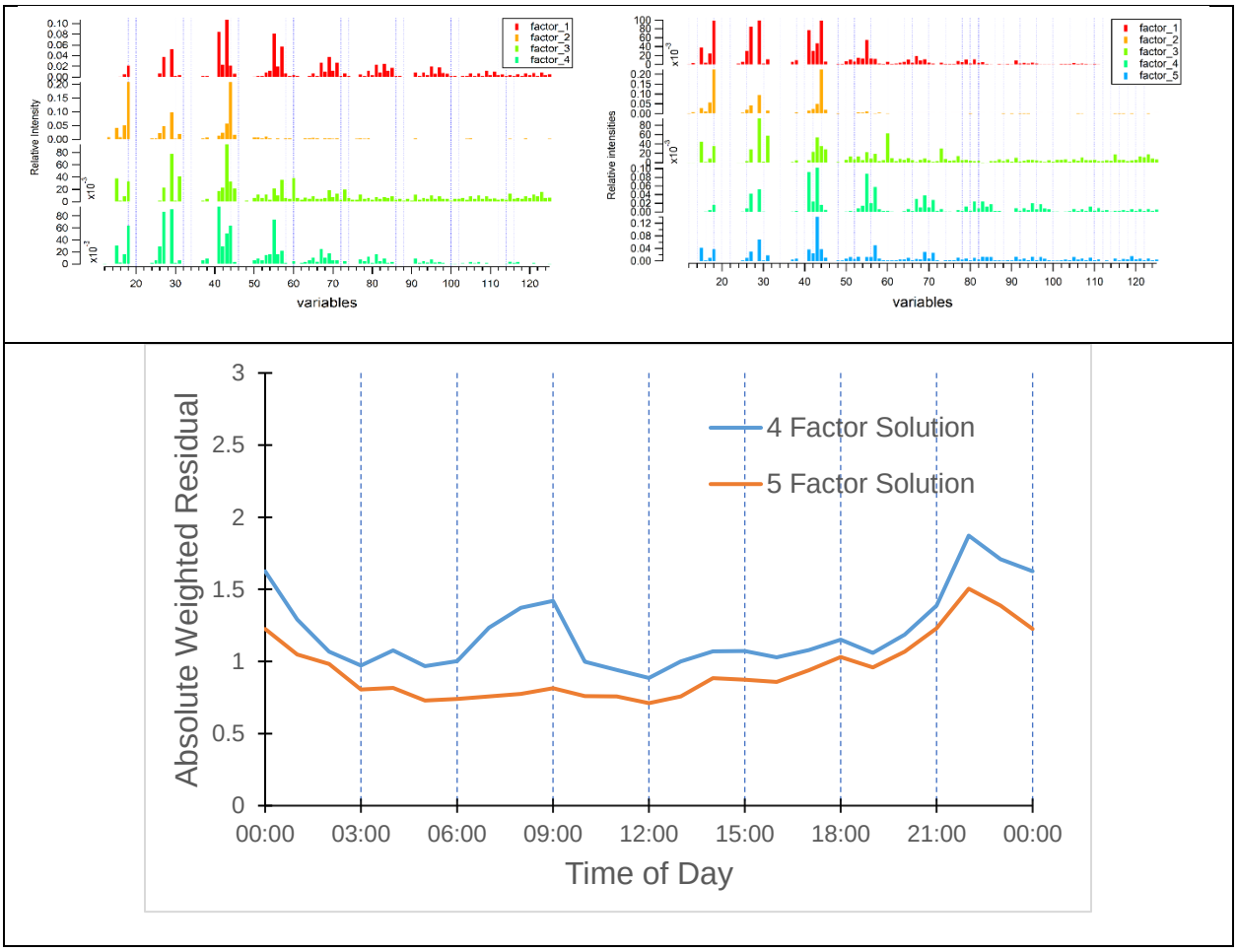

Figure S5. Four factor unconstrained PMF run for the cold season of 2016 – 2017 is shown in the upper left panel. The five factor PMF solution is presented in the upper right panel. Diurnal variability of the Absolute Residual weighted over uncertainty for both solutions m/z=55 fragment is presented in the lower panel.

2017 Warm period: For the warm period, given the absence of significant signal at the two key biomass burning fragments at m/z=60 and m/z=73, a five factor solution containing a biomass burning factor was not anticipated. Nevertheless, four and five factor solutions were examined and resulting FPs are presented in figure SF.6. As can be seen the four factor solution is able to predict what could be an HOA – like factor in position two, heavily impacted though by the fragment of CO_2^+ at m/z=44, a COA – like factor in position 1, exhibiting the expected difference in relative intensities between m/z=55 and m/z=57, plus two SOA factors, one resembling a highly oxygenated product at position 4 and an SV-OOA like spectrum at position 3. When going through the five factor run some splitting behavior can be observed. An environmentally irrelevant factor immerges at position 4, while no satisfactory profile can be seen for any primary factor,

either HOA or COA. Consequently, the four factor solution will be explored on the next step of the SA procedure.

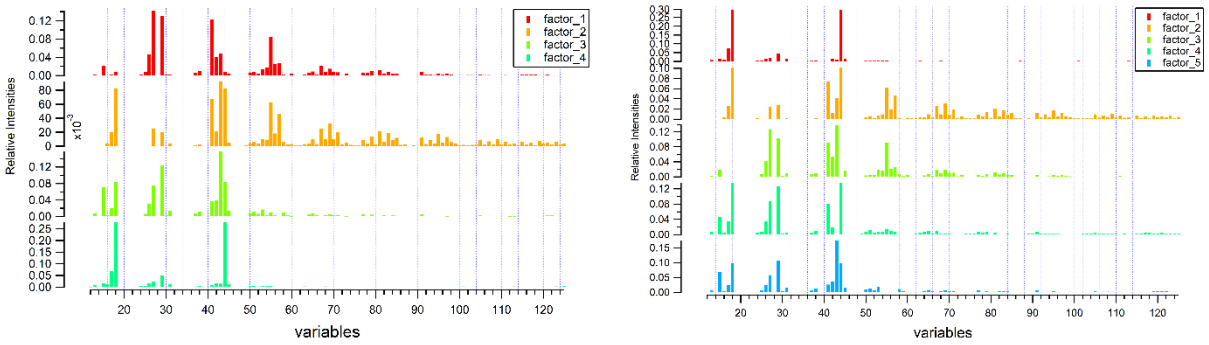

Figure S6. Factor profiles for the four (left) and five (right) factor unconstrained runs for the 2017 warm period dataset.

S4.3 HOA constrained runs

Proceeding to the second step of the SA method, a constrain is introduced for one of the factors, using as an RFP the average HOA profile obtained by Ng et al. (2011).

Cold Period 2016-2017: In the left panel of Figure SF.7 the obtained FPs are presented. As can be seen, a BBOA – like factor with contributions from m/z=60 and m/z=73 emerges in position 3. A COA – like factor can be seen in position 5. Two SOA factors, with a contribution at m/z=44 seem to also appear in positions 2 and 4.

2017 Warm period: The solution obtained when constraining the HOA factor at position 1 is presented in the right panel of Figure SF.7. It is apparent that this model configuration leads to a COA – like factor in position 2 and two SOA factors exhibiting different levels of oxidation. In the next step the optimum solution is obtained by constraining the COA factor as well.

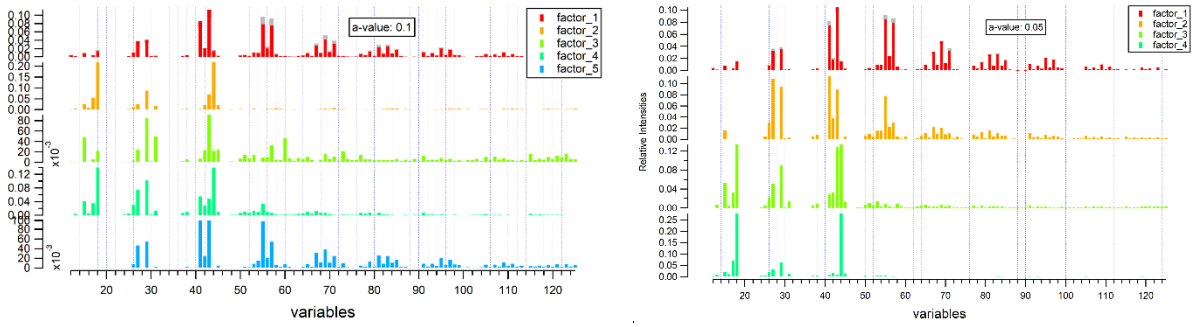

Figure S7. Five factor run with HOA constrained (a=0.1) at position 1 for the cold period of 2016 – 2017 depicted on the left panel. On the right panel, the HOA constrained solution for the warm 2017 period.

S4.4 HOA – BBOA constrained runs

This step is performed for the winter – time datasets. When constraining two factors, one using the average HOA spectrum from Ng et al. (2011) and the second using the BBOA spectrum obtained in the same study, the five factor solution indicatively for the 2016 – 17 cold period, is presented in Figure SF.8. This step has been implemented for all winter – time datasets, with similar results. As is evident in position three a primary factor resembling COA emerges once more. The model exhibits low seed variability while an oxidized factor with considerable contribution at m/z 60 and 73 emerges in position 5.

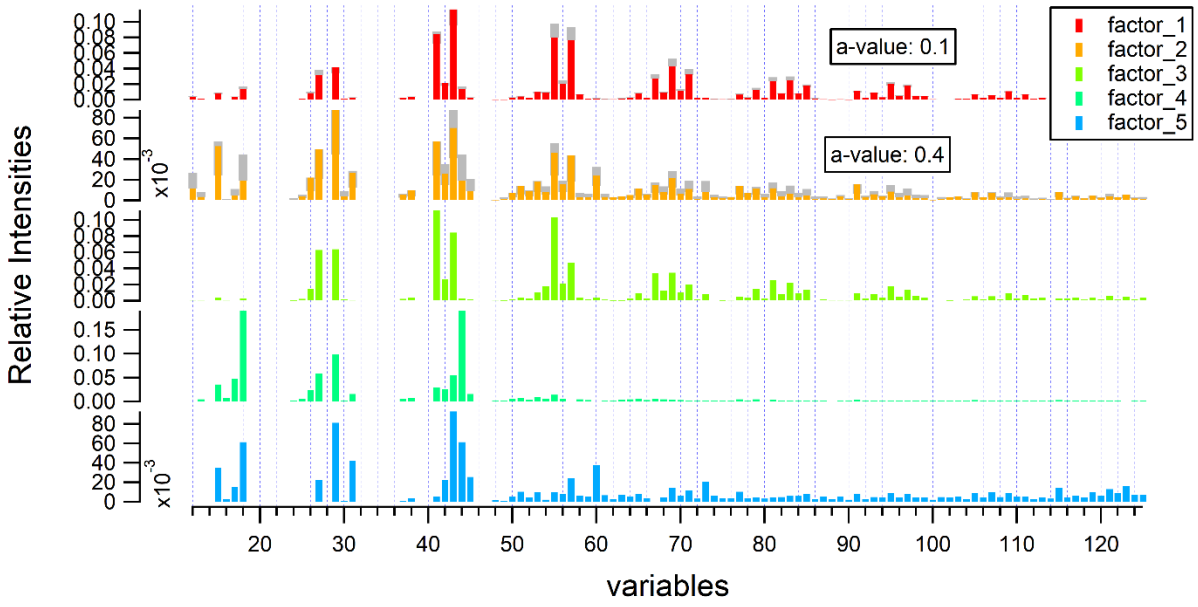

Figure S8. Five factor solution constraining HOA and BBOA for the cold period of 2016 – 2017.

When replicating the methodology of Mohr et al. (2012) (Figure SF.9) for the same period, data points corresponding to early afternoon (~16:00) and the evening lie closer to the linear fit slopes representing COA factors indicating the presence of cooking – like aerosol affecting the measuring site. On the other hand, data obtained during the time frame of the morning rush hour border on the reference line of HOA.

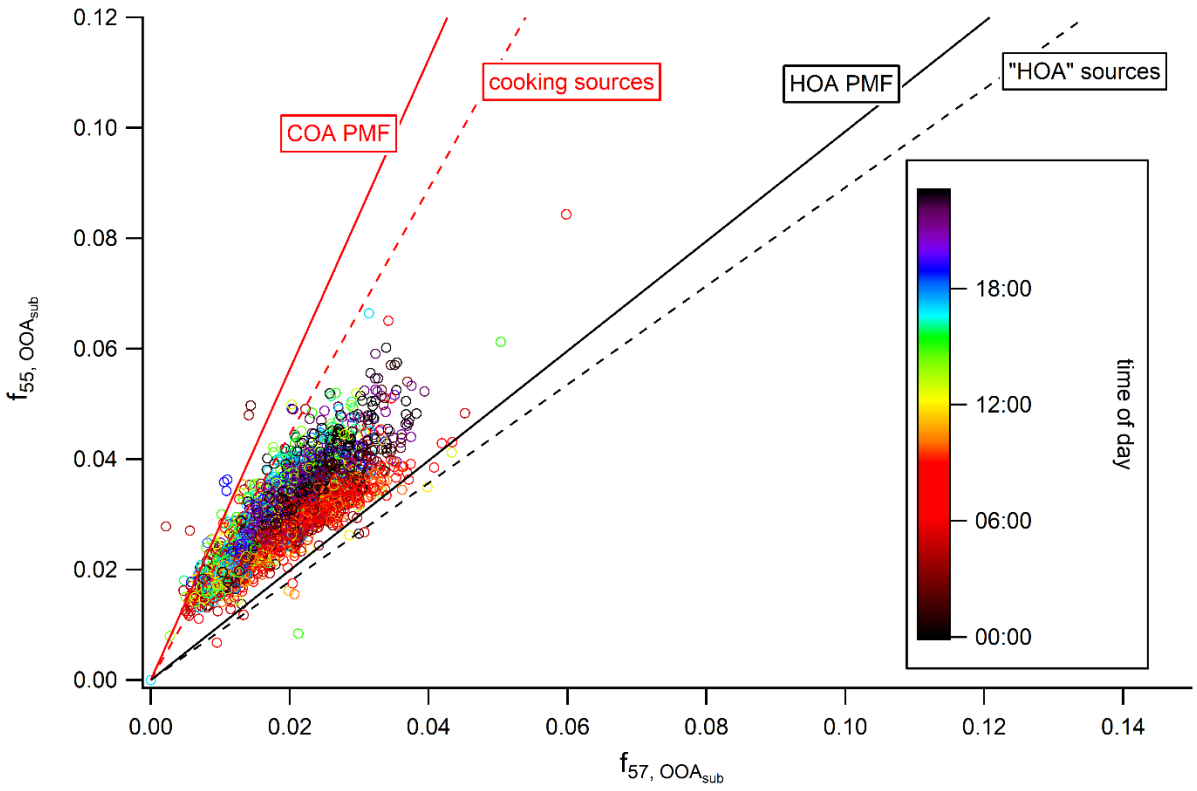

Figure S9. $f_{55,\ OOAsub}$ plotted against $f_{57,\ OOAsub}$ indicatively for the 2016 – 2017 cold period. Data points are colored according to time of day. Lines correspond to linear fit results conducted using COA and HOA results both from PMF and laboratory standards studies (Mohr et al., 2012).

S4.5 Sensitivity analysis on the α value

When proceeding to the final step of the SA procedure, three constrains are implemented for the cold period datasets (HOA, BBOA, COA) and two (HOA, COA) for the warm period datasets. Three scenarios of different levels of constrains applied to the primary OA factors and the respective impact on the relative contribution of each factor have been tested in an effort to minimize subjectivity introduced by the degree of freedom left for the model to vary around the RFP used. The α values ranged from 0.05 to 0.1 with an increment of 0.025 for the HOA factor (Crippa et al.,2014), from 0.1 to 0.2 (Canonaco et al., 2015) with an increment of 0.05 for COA for all the datasets handled. For BBOA the examined range was for α values varying from 0.3 to 0.5 with an increment of 0.1 and was tested for the cold season datasets. As indicatively exhibited in Figures SF.10 and SF.11 no considerable variability was observed for both the cold and warm period datasets, where maximum fractional difference of contributions was found to be less than 5%.

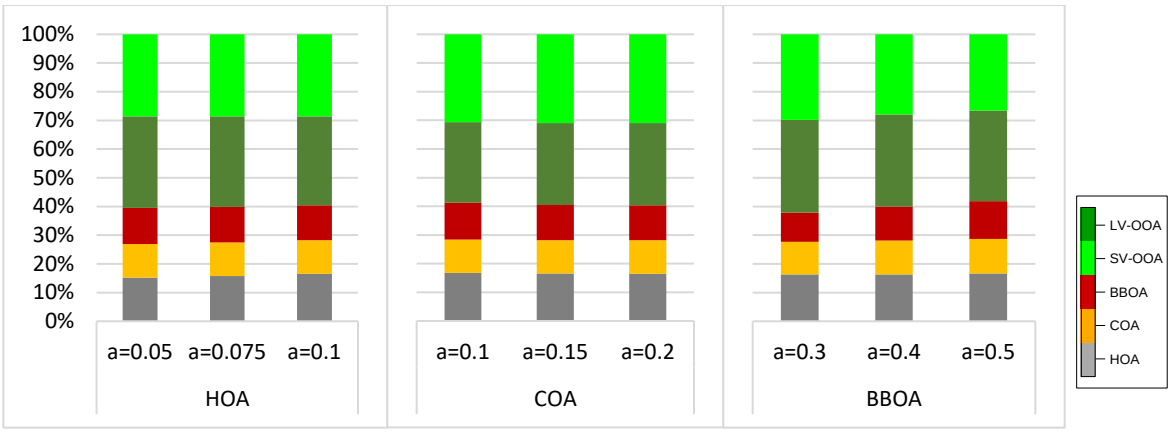

Figure S10. Relative contribution of each deconvolved factor for varying α values regarding HOA, COA and BBOA for the winter 2016 – 17 dataset.

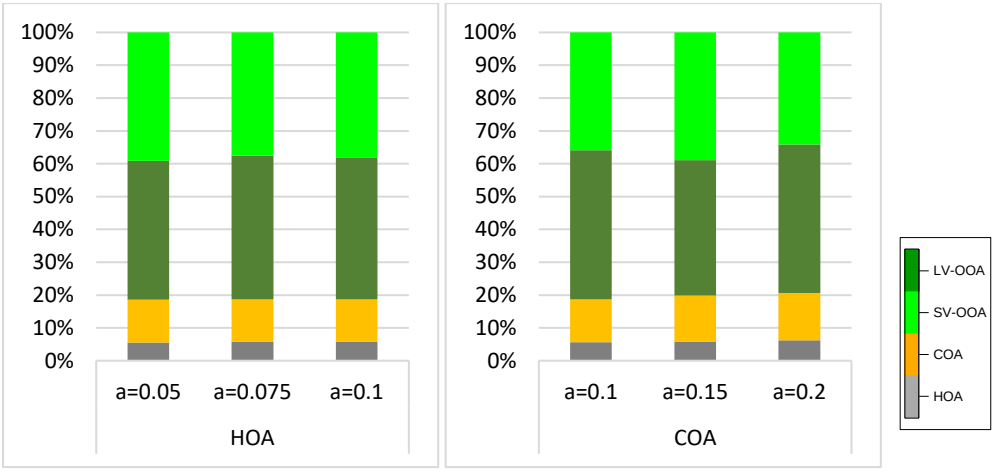

Figure S11. Relative contribution of each deconvolved factor for varying α values regarding HOA and COA for the warm period of 2017.

S 4.6 Mass spectra of the selected solutions

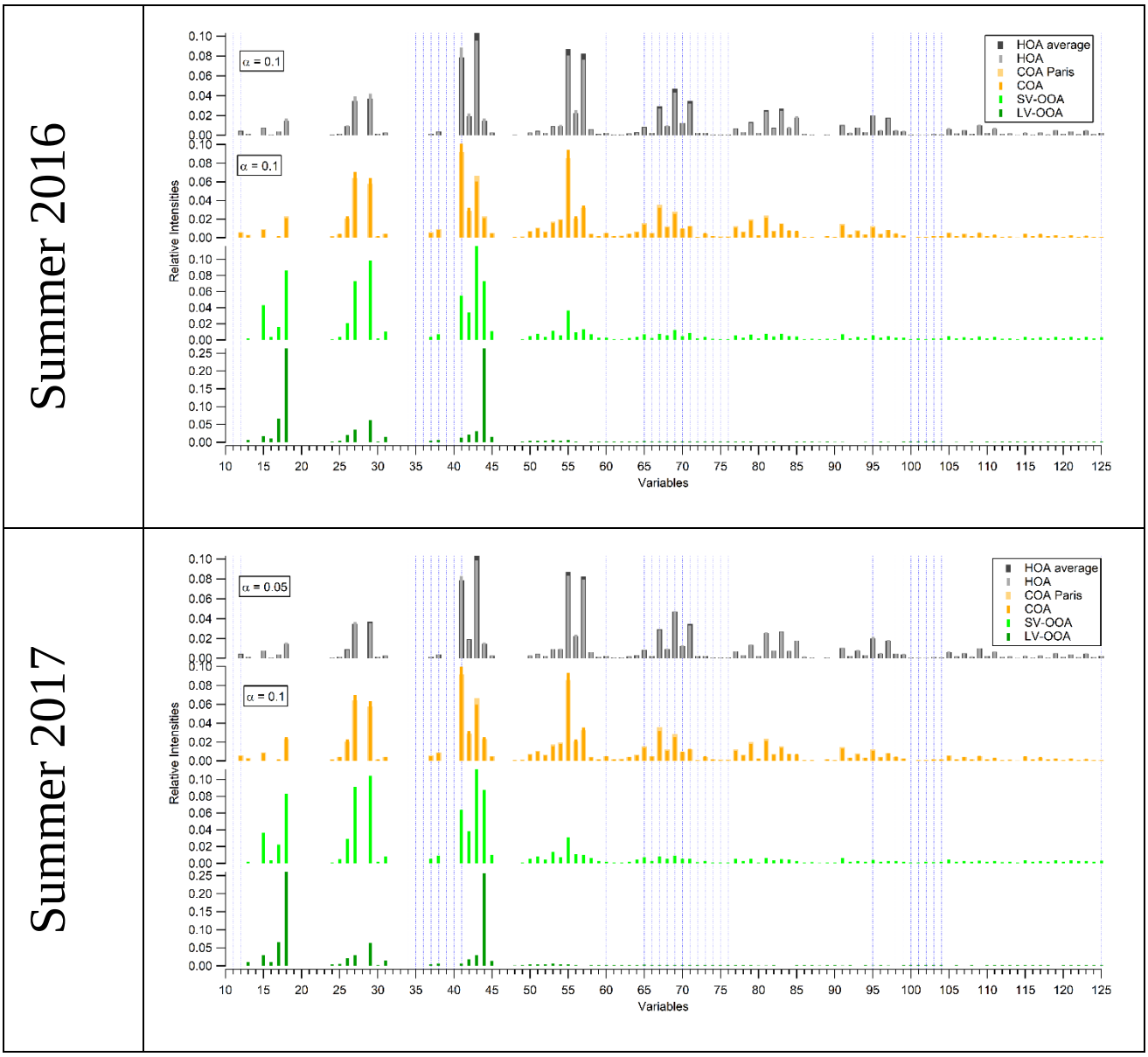

Figure S12. Mass spectra of the derived PMF Factors and reference spectra used, together with the corresponding α-values for the two studied summer periods.

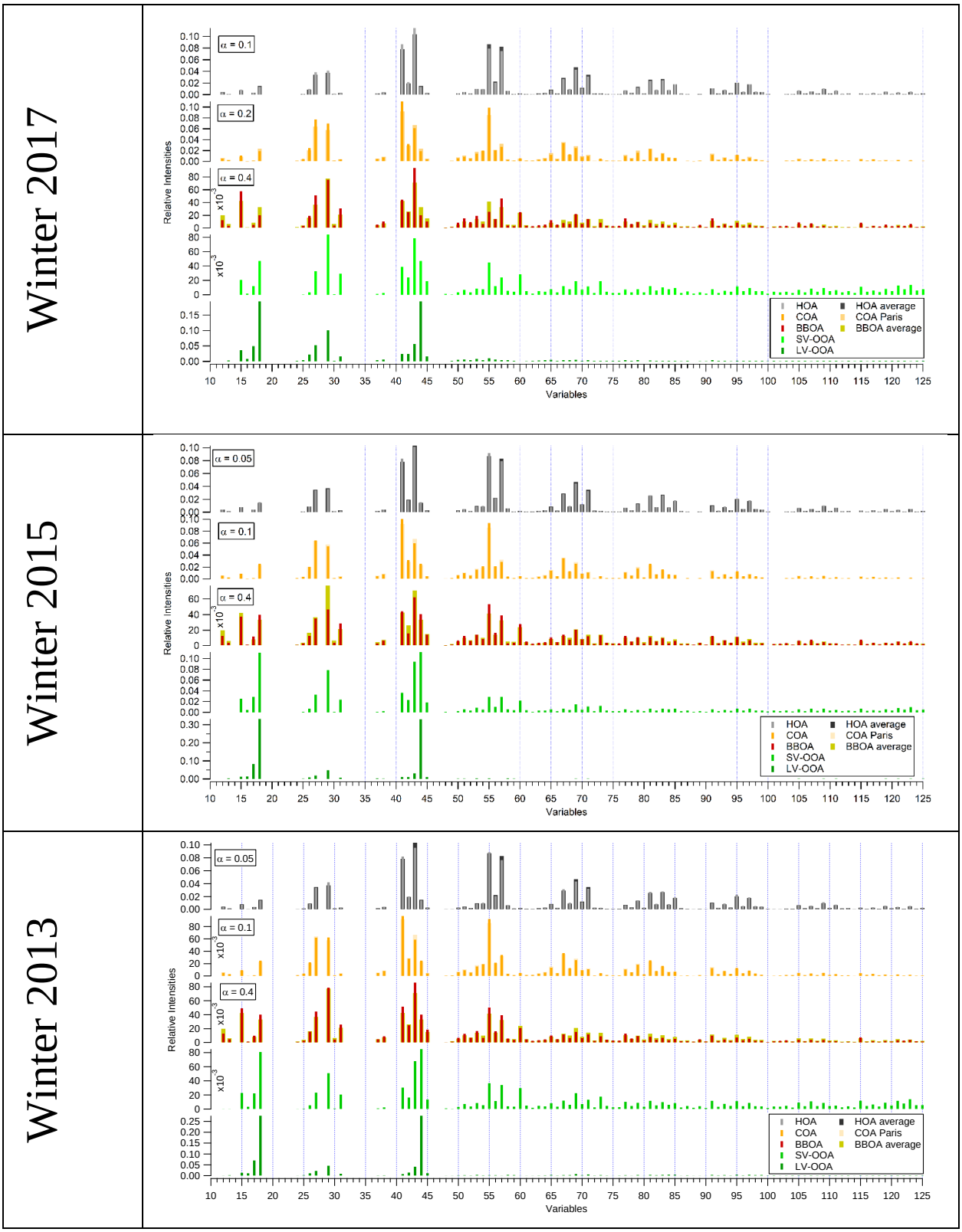

Figure S13. Mass spectra of the derived PMF Factors and reference spectra used, together with the corresponding α-values for the three studied winters.

S4.7 Model residuals for the selected solutions

For the selected solutions, residuals weighted over uncertainty analysis and Organics concentration reconstruction, as resulting from the sum of the different PMF Factors is provided in the following figure.

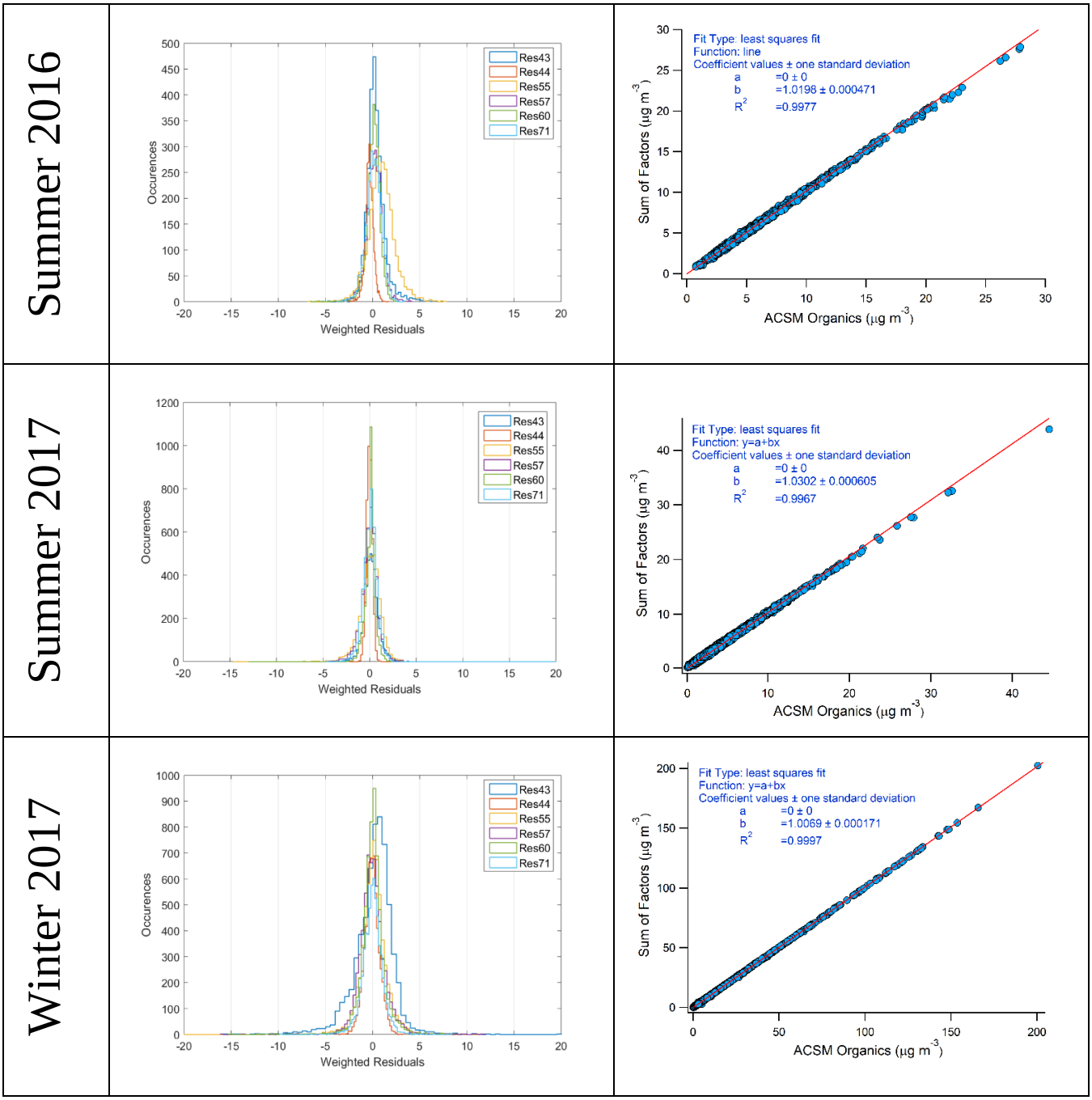

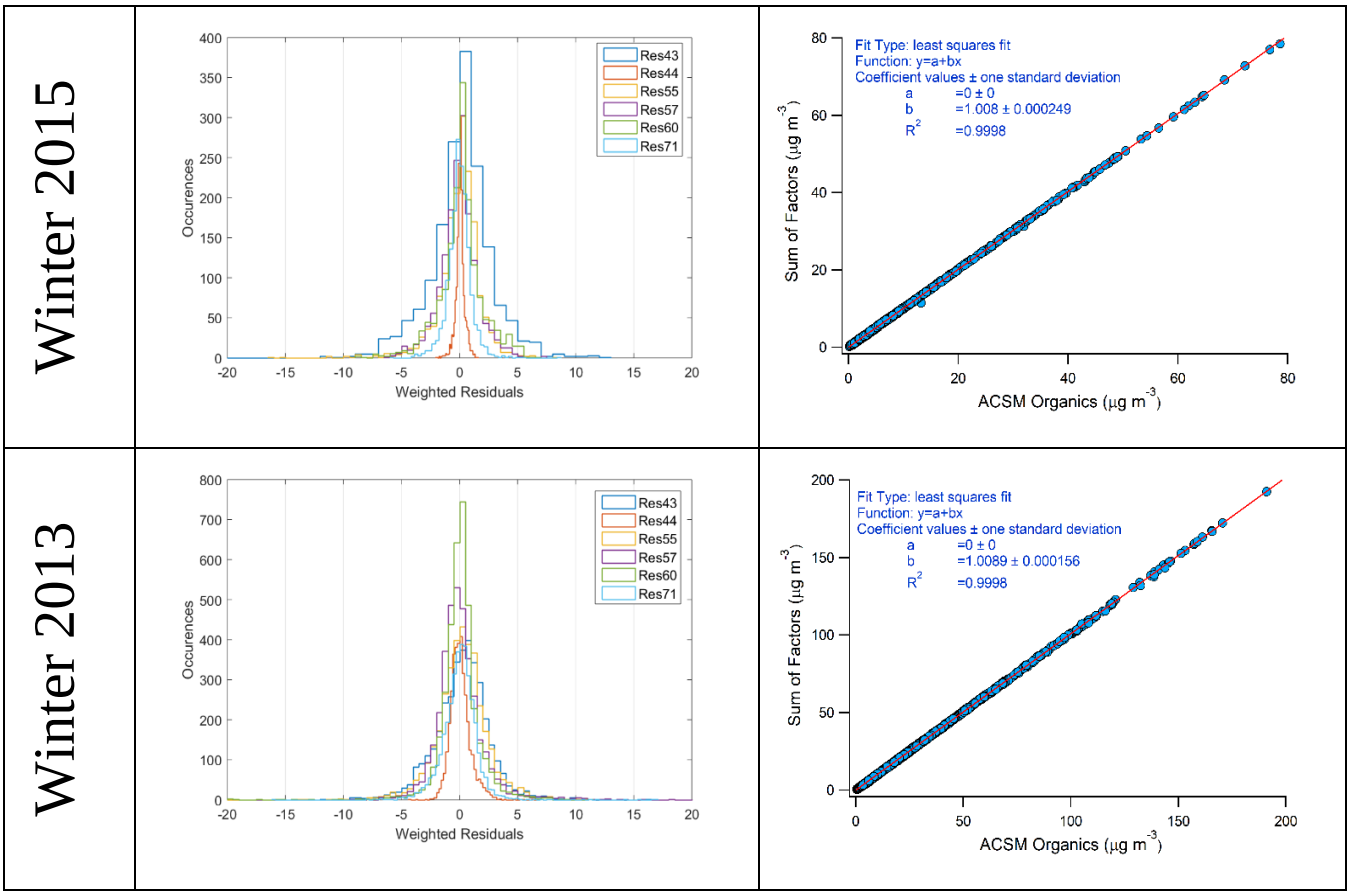

Figure S14. Histograms of weighted residuals for variables m/z 43, 44, 55, 57, 60, 71 of the selected solutions and comparison of the sum of the PMF Factors with the Organics measured by the ACSM.

S4.8 Affinity of obtained spectra with literature mass spectra

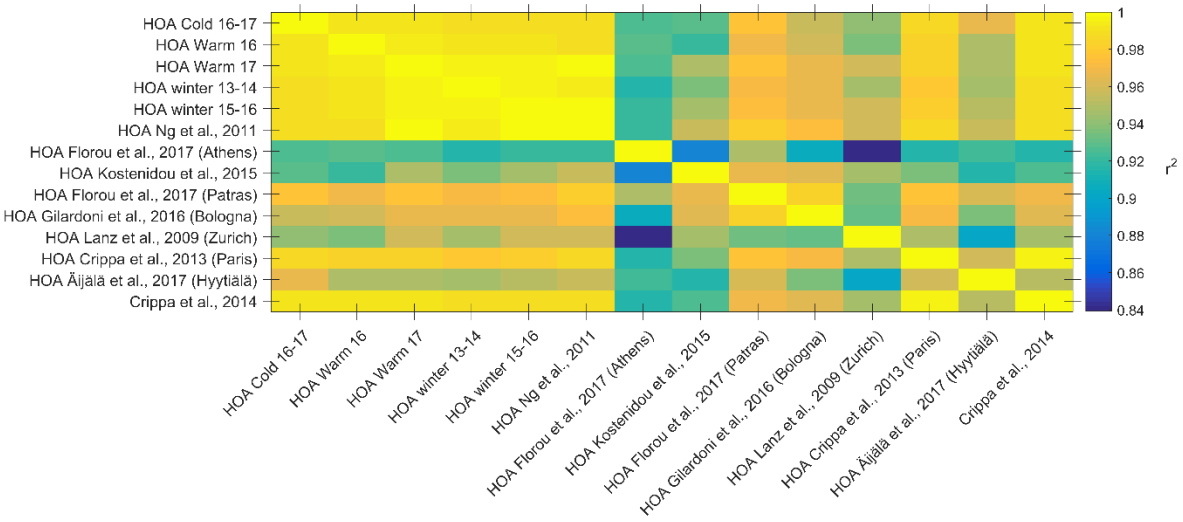

Figure S15. Coefficient of determination for linear regression (r^2) of deconvolved HOA profiles from this study versus literature spectra. Note range of color scale.

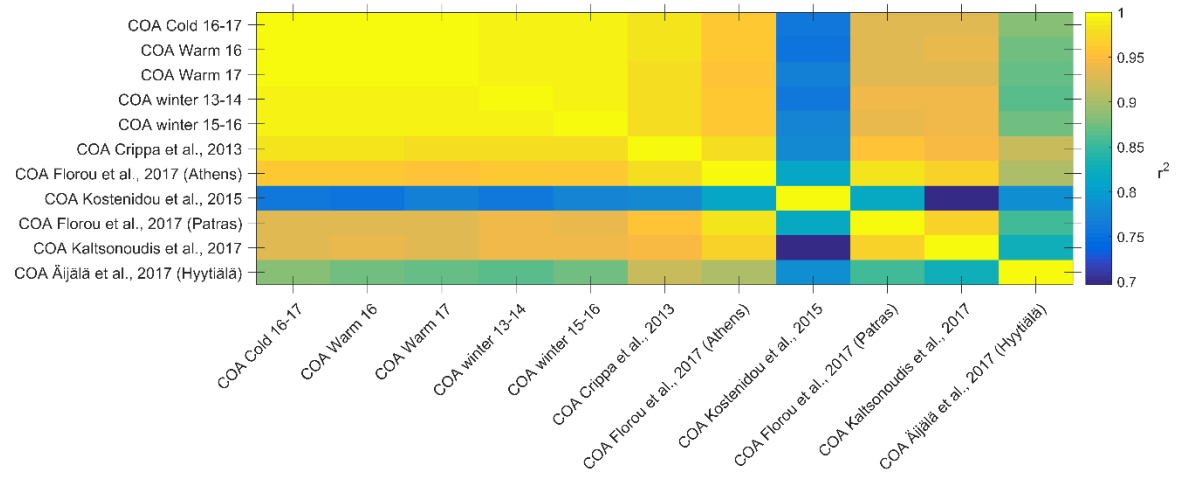

Figure S16. Coefficient of determination for linear regression (r^2) of deconvolved COA profiles from this study versus literature spectra. Note range of color scale.

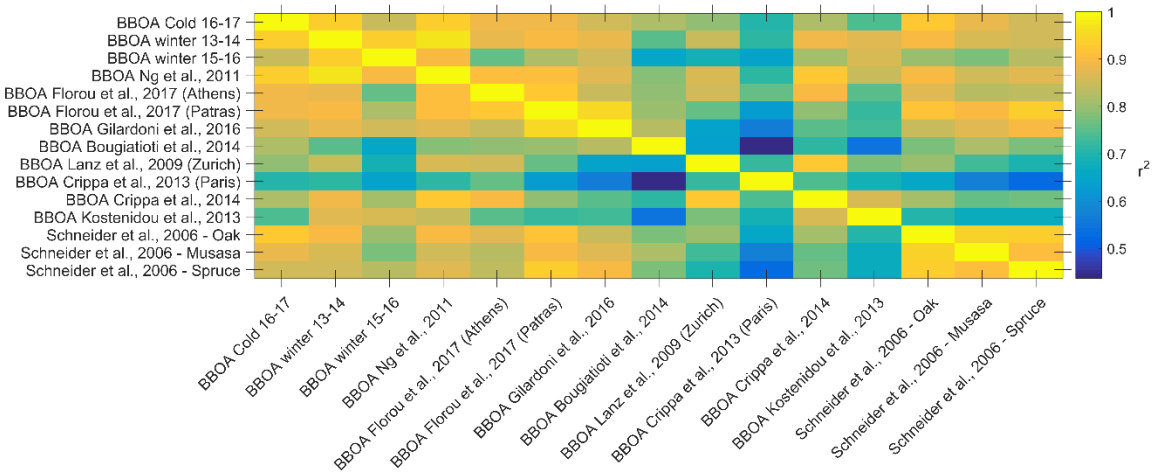

Figure S17. Coefficient of determination for linear regression (r^2) of deconvolved BBOA profiles from this study versus literature spectra. Note range of color scale.

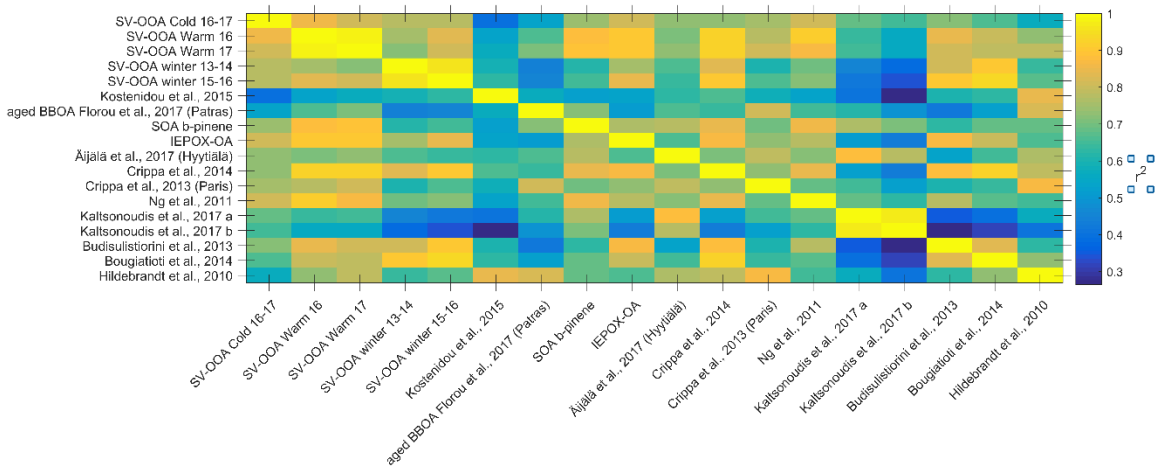

Figure S18. Coefficient of determination for linear regression (r^2) of deconvolved SV-OOA profiles from this study versus literature spectra. Note range of color scale.

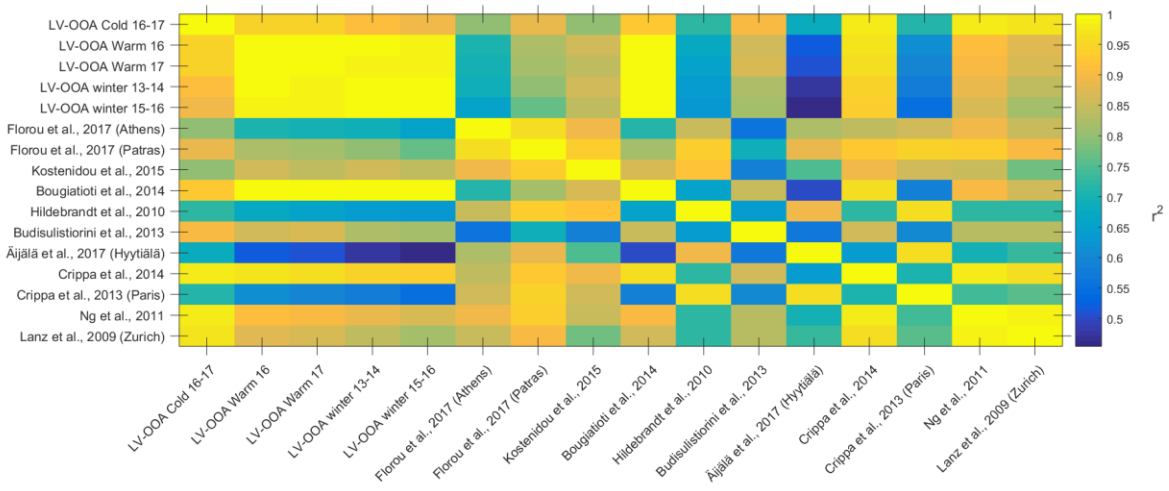

Figure S19. Coefficient of determination for linear regression (r^2) of deconvolved LV-OOA profiles from this study versus literature spectra. Note range of color scale.

S4.9 Correlation of obtained factor timeseries with independent measurements

r^2	BC	BC_{wb}	BC_{ff}	CO	nss-K^+	SO_4^{2-}	NO_3^-	NH_4^+	Cl
HOA	0.65	0.52	0.60	0.65	0.32	0.22	0.30	0.26	0.54
COA	0.39	0.36	0.32	0.33	0.34	0.11	0.22	0.15	0.35
BBOA	0.56	0.77	0.24	0.51	0.55	0.12	0.35	0.19	0.61
SV-OOA	0.77	0.90	0.44	0.73	0.55	0.21	0.38	0.26	0.80
LV-OOA	0.26	0.18	0.27	0.21	0.40	0.36	0.61	0.58	0.27

Table S2. Coefficients of determination r^2 of the factor timeseries obtained against independent measurements for the cold period of 2016 – 2017.

r^2	CO	BC_{wb}	BC_{ff}	BC	NO	NO_2	SO_4^{2-}	NO_3^-	NH_4^+
HOA	0.44	0.50	0.63	0.64	0.47	0.13	0.02	0.62	0.02
COA	0.33	0.19	0.12	0.13	0.08	0.24	0.05	0.36	0.05
SV-OOA	0.40	0.37	0.34	0.35	0.19	0.26	0.22	0.86	0.24
LV-OOA	0.04	0.08	0.06	0.07	0.01	0.02	0.62	0.34	0.63

Table S3. Coefficients of determination r^2 of the factor timeseries obtained against independent measurements for the 2017 warm period

S5 Influence of wind speed/direction and of air masses origin

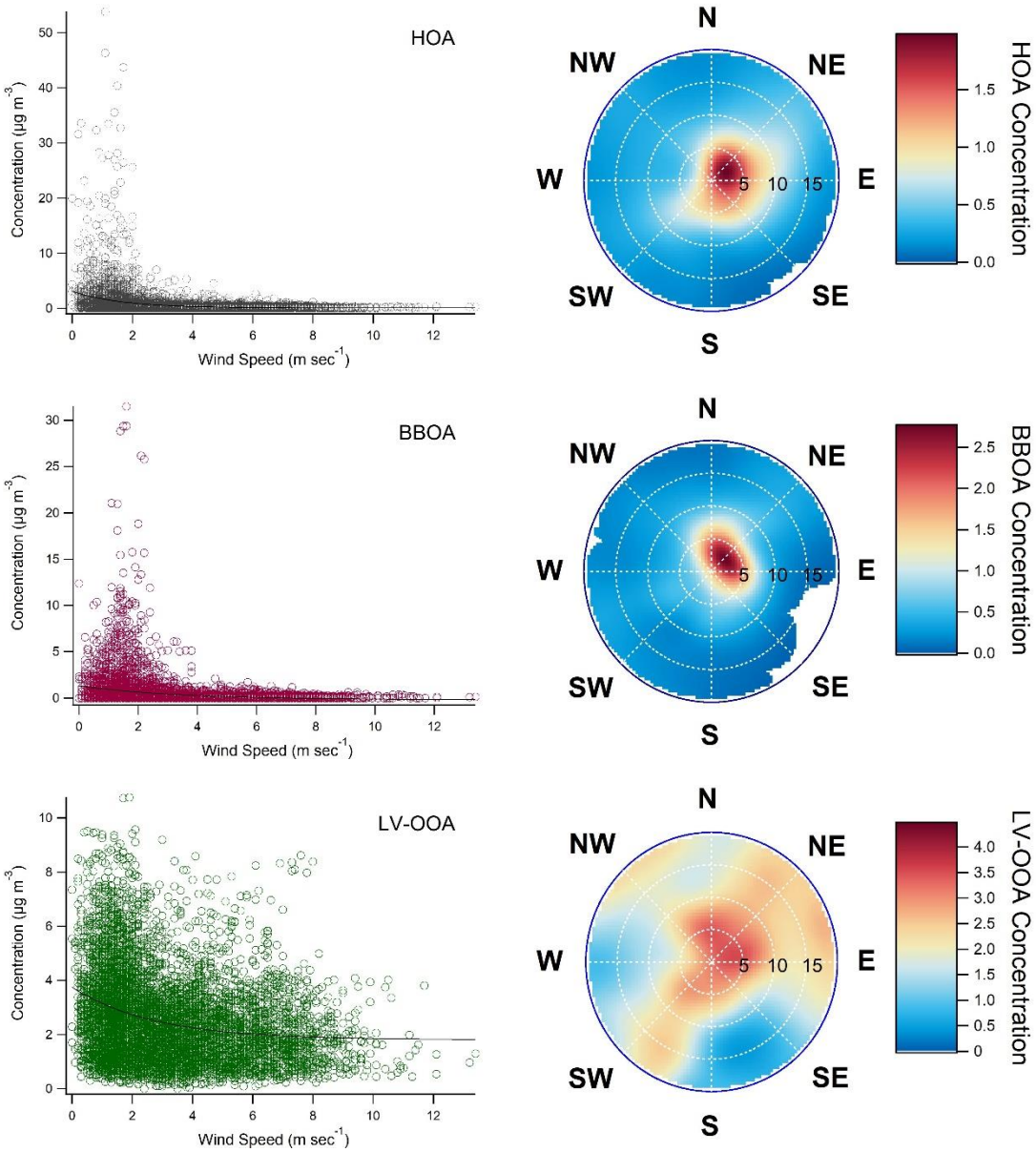

Figure S20. Indicative wind analysis results for organic aerosol components in Athens. On the left, hourly averaged concentration vs. wind speed scatterplots. On the right, respective bivariate (wind speed-direction) polar plots for hourly averaged concentrations. The radial axis (wind speed) in km h^{-1}.

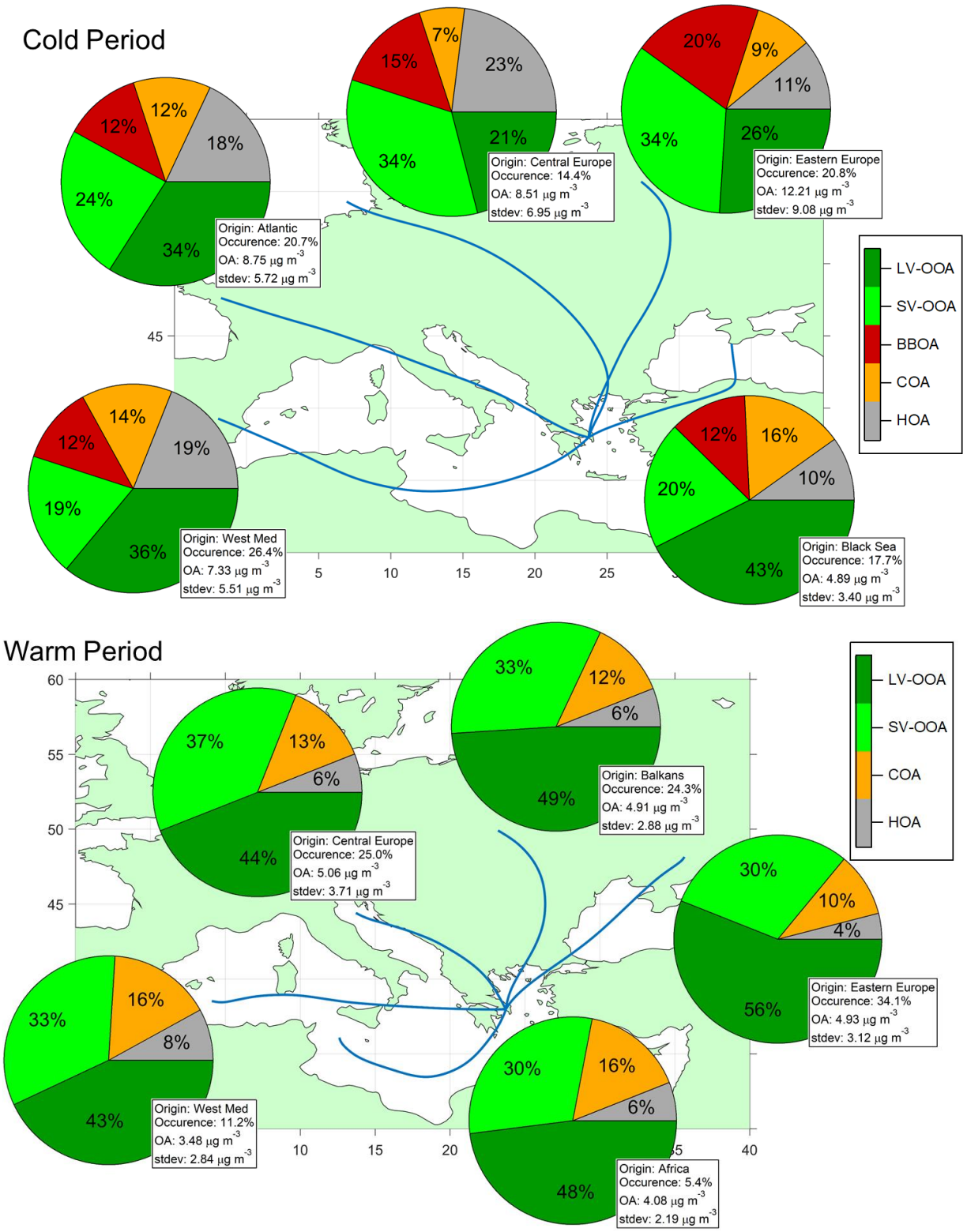

Figure S21: Average compositional pie-charts of OA fractions for each trajectory cluster, separately for cold (November 2016 – March 2017) and warm (Aug-Sep 2016 and May-Jul 2017) periods on the top and bottom panel respectively. Displaying also frequency of occurrence and average OA concentrations for each cluster.